crystals

MDPI

Article

Growth and Property Investigations of Two Organic–Inorganic Hybrid Molecular Crystals with High Thermal Stability: 4-Iodoanilinium perchlorate 18-crown-6 and 4-Iodoanilinium borofluorate 18-crown-6

Lihui Zhang [1], Tiantian Kang [1], Fanghua Zhao [2], Duanliang Wang [1], Chuanying Shen [1,*] and Jiyang Wang [3]

1 Shandong Province Key Laboratory of Laser Polarization and Information Technology, School of Physics and Engineering, Qufu Normal University, Qufu 273165, China; zlh4362@163.com (L.Z.); kangtian_03@163.com (T.K.); wdliang012@163.com (D.W.)
2 School of Chemistry and chemical Engineering, Qufu Normal University, Qufu 273165, China; zfh101@163.com
3 State Key Laboratory of Crystal Materials, Institute of Crystal Materials, Shandong University, Jinan 250100, China; jywang@sdu.edu.cn
* Correspondence: shenshouchuan@163.com

Received: 15 March 2019; Accepted: 11 April 2019; Published: 15 April 2019

Abstract: Two new organic–inorganic hybrid molecular single crystals, 4-Iodoanilinium perchlorate 18-crown-6 (**1**) and 4-Iodoanilinium borofluorate 18-crown-6 (**2**), with large sizes and high thermal stability were successfully synthesized by solution method. Their structures, phase purities, thermal stability, dielectric, absorption and fluorescence spectra were systematically investigated for potential applications. Compounds 1 and 2 crystallize in orthorhombic crystal system, in same space group, namely Pnma. The thermal measurements shown **1** and **2** maintain high thermal stability up to 150 °C. The temperature dependency of dielectric constant was studied, and no distinct anomaly was observed. The band gap were calculated to be 3.38 eV and 3.57 eV for **1** and **2**, respectively, slightly smaller than those of layer perovskite (benzylammonium)$_2$PbCl$_4$ semiconducting materials, which have potential applications in optoelectronic detection field. The investigations throw light on the semiconductor properties of organic–inorganic hybrid crown type material and provide two types of crown compounds with high thermal stability.

Keywords: crystal growth; organic–inorganic hybrid; supramolecular single crystals; optical properties; high thermal stability

1. Introduction

Recently, much attention has been drawn to organic–inorganic hybrid molecular crystals materials [1–11]. These materials are frequently characterized by their various physical and chemical properties, such as structural phase transition, ferroelectric, semiconductor, photovoltaic effect, nonlinear optical response and pyroelectricity, which have potential applications in molecular sensors, switches, data storage, electro optical modulators, light emitting, photo-detector, energy-efficient memories, filtering devices, high-performance insulators and so on [12–22]. Among them, an interesting class is the organic–inorganic hybrid crown type, owing to their large group of structural diversities as well as unique properties (such as dielectric anomaly, ferroelectric, second harmonic generation, nonlinear optical properties, etc.) [23,24].

A large number of crown type molecular materials have been synthesized in the recent decades [23–34]. For example, 4-methoxyanilinium tetrafluoroborate-18-crown-6 shows a second-order ferroelectric phase transition at 127 K, together with an abrupt dielectric anomaly, Debye-type relaxation behaviour [24]. Methoxyanilinium perrhenate 18-Crown-6 undergoes disorder–order structural phase transition at about 153 K, with ferroelectric spontaneous polarization was determined to be 1.2 μC/cm^2 [25]. (2,6-diisopropylanilinium)([18]crown-6)](ClO_4) underwent a sequence of phase transitions (Ibam-Pbcn-Pna21) at T_1 = 278 K and T_2 = 132 K, with a saturation polarization of 0.35 μC/cm^2 obtained at 108 K [26]. [(2,6-diisopropylanilinium)([18]crown-6)]BF_4 go through two phase transitions at T_1 = 305 K and T_2 = 120 K, and P_s and P_r reaching about 0.3 and 0.25 μC/cm^2 at 100K, with a large dielectric anomaly, significant pyroelectricity, and SHG response appeared [27]. Bis(imidazolium hydrochlorate) dehydrate 18-crown-6 displays attractive switching performances with a superior second-order nonlinear optical switching contrast (calculated by Landau theory) of 12 at about 0 K, and a phase transition occurred at 220 K [28]. (4-HNA)(18-crown-6)(HSO_4) underwent phase transition at about 255 K with space group of $P2_1/c$ in the high-temperature phase and $P2_1/n$ in the low-temperature phase [29]. [(3-nitroanilinium+)(18-crown-6)][IO_4](CH_3OH) was discovered displaying dielectric anomalous behaviors at phase temperature of 220 K, with space group of C2/c both before and after phase transition [30].

However, most of the phase-transition/decomposition temperatures of hybrid molecular crystals of crown system were reported occurred at low temperatures. From a practical point of view, such transition take place at low temperature imposes important limitation for potential applications. Therefore, in this work, two organic–inorganic hybrid supramolecular crystals with high phase-transition temperatures, 4-Iodoanilinium perchlorate 18-crown-6 ($C_6H_7IN^+ \cdot ClO_4^- \cdot C_{12}H_{24}O_6$) (**1**) and 4-Iodoanilinium borofluorate 18-crown-6 ($C_6H_7IN^+ \cdot BF_4^- \cdot C_{12}H_{24}O_6$) (**2**), were successfully grown by solution method. Their physical properties, including in structures, phase purities, phase transitions, dielectric, absorption and fluorescence spectra were firstly systematically investigated for potential applications.

2. Materials and Methods

Compared with traditional/routine methods (such as Czochralski method, flux method and Bridgman method), the solution method have many advantages, including low cost, low growth temperature, easy observations, easy to produce large size crystals and so on. Therefore, in this work, crystals **1** and **2** were obtained by solution method—that is after the solute were dissolved in solvent, by naturally volatilizing solvent at room temperature, the solution become oversaturate solution, and then crystals **1** and **2** could be grown slowly from the above oversaturate solution. All reagents and solvents in the syntheses were of reagent grade and used without further purification. Stoichiometric ratio of 18-crown-6, 4-iodoaniline and $HClO_4$/HBF_4 were dissolved in acetone solutions to synthesize crystals **1** and **2**. The synthetic process and molecular configurations of the two crystals are shown in Scheme 1.

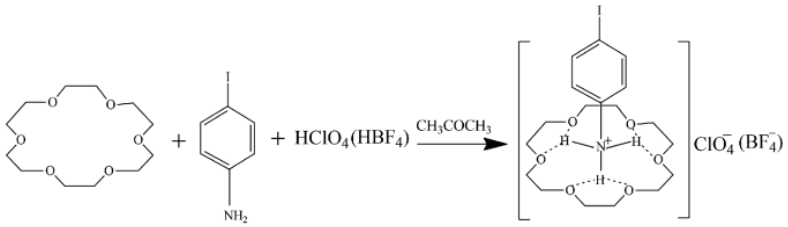

Scheme 1. The synthetic process and molecular configurations of crystals **1** and **2**.

Infrared spectra were obtained using a Nicolet Magna-IR 560 infrared spectrometer and KBr pellets in the 4000–400 cm^{-1} region to confirm the phase purity.

Single-crystal X-ray data of the as-grown crystals were collected on a Bruker SMARTAPEX II CCD with Mo-Kα radiation (λ = 0.71073 Å) at 153 K. The structures of crystals **1** and **2** were solved by direct methods and refined by full-matrix method based on F^2 by means of SHELXLTL software package. Besides, phase purities were also checked by powder X-ray diffraction (XRD), using a Bruker-AXS D8 ADVANCE X-Ray diffractometer with Cu-Kα1 radiation (λ = 1.54186 Å) in the ranges of 10°–50° (2θ) with a time setting of 0.1 s per step and a step length of 0.002°.

Thermal measurement is commonly used to detect whether a compound displays a phase transition triggered by temperature. In this work, the Differential Scanning Calorimetry (DSC) and Thermogravimetric Analysis (TG) data were recorded using a NETZSCH STA 449F3 instrument from −150 °C to 250 °C with a heating rate of 10 °C/min under nitrogen at atmospheric pressure in aluminum crucibles.

The variable-temperature dielectric response is another common method for detecting phase transitions. The complex dielectric permittivity ε ($\varepsilon = \varepsilon' - i\varepsilon''$) was measured on pressed-powder pellets that were covered by silver conducting glue. An Impedance E4990A analyzer was used to record the variability of ε' of crystals **1** and **2** in the frequency between 1 kHz and 500 kHz from −175 °C to 100 °C.

The optical properties, including absorption and fluorescence measurements were carried out at room temperature. By grinding the air-dried crystals into fine powder, the polycrystalline samples were prepared to measure the UV-vis absorption spectra on a UV-2700 spectrometer with an integrating sphere over the spectral ranges of 175–850 nm. The photoluminescence (PL) spectra was performed by employing an FLSP-920 fluorescence spectroscopy (Edinburgh Instruments) using a Xenon lamp with 300 nm excitation the as-grown single crystals.

3. Results

3.1. Crystal Growth

Large transparent and colorless single crystals of **1** and **2** were obtained by slow evaporation solution, as shown in the inset of Figure 1. Figure 1 also illustrate the Infrared (IR) spectra of the as grown crystals **1** and **2**: 3432(s), 2913(s), 1352 (s), 1692(s), 1492 (s), 1975(w), 835 (s), 1299(s), 1250(s), 1021(s).

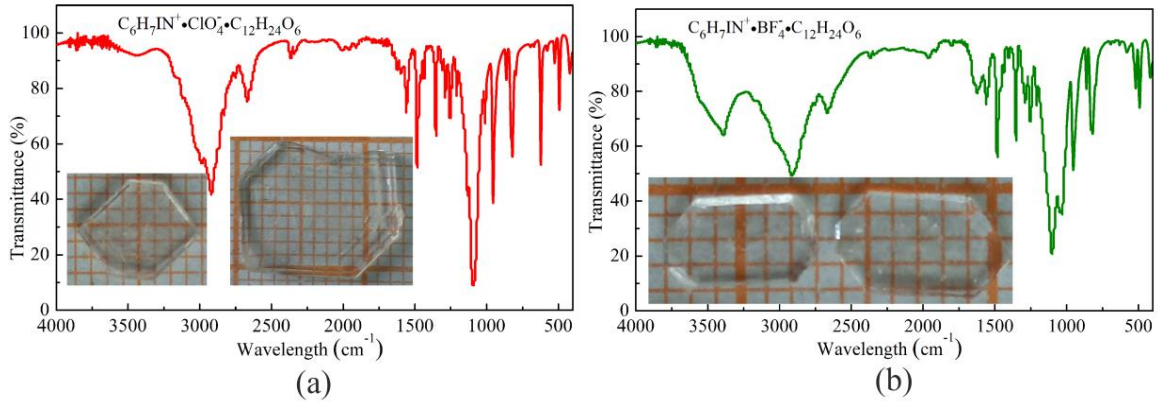

Figure 1. The as-grown crystals and the Infrared (IR) spectra of (**a**) $C_6H_7IN^+ \cdot ClO_4^- \cdot C_{12}H_{24}O_6$ and (**b**) $C_6H_7IN^+ \cdot BF_4^- \cdot C_{12}H_{24}O_6$.

3.2. Crystal Structure and XRD

Crystallographic data and structure refinements of crystals **1** and **2** are listed in Table 1. Both the two crystals crystallized in orthorhombic with space group of Pnma. The lattice parameters a, b, c and cell volume V were calculated to be 15.975(3) Å, 11.418(2) Å, 12.743(3) Å and 2324.4(8) $Å^3$ for compound **1**, and 15.901(3) Å, 11.289(2) Å, 12.735(3) Å and 2286.0(8) $Å^3$ for compound **2**, respectively.

Table 1. Summary of crystallographic data for crystals **1** and **2** at 150 K.

Empirical Formula	$C_{18}H_{31}ClINO_{10}$	$C_{18}H_{31}BF_4INO_6$
formula weight/g·mol^{-1}	583.79	571.15
temperature/K	153	153
wavelength/Å	0.71073	0.71073
crystal colour	Colourless	Colourless
crystal system	Orthorhombic	Orthorhombic
space group	Pnma	Pnma
a/Å	15.975(3)	15.901(3)
b/Å	11.418(2)	11.289(2)
c/Å	12.743(3)	12.735(3)
α/°	90	90
β/°	90	90
γ/°	90	90
volume/Å^3	2324.4(8)	2286.0(8)
Z	4	4
density/mg·m^{-3}	1.668	1.660
Absorption coefficient (mm^{-1})	1.545	1.467
F(000)	1184	1152
Measured theta range (°)	3.01~27.45	3.02~27.48
Absorption correction	Semi-empirical from equivalents	
Data/restraints/parameters	2787/0/154	2753/0/155
GOF on F^2	1.004	1.012
R, wR [I > 2sigma(I)]	0.0380, 0.1025	0.0268, 0.0804
R, wR [all data]	0.0400, 0.1042	0.0287, 0.0818
CCDC	1883445	1883437

The crystal structure of compound **1** was described as a representative. As depicted in Figure 2a, the asymmetric unit consists of one [(4-Iodoanilinium)(18-crown-6)]$^+$ cation and one ClO_4^- anion. The 4-Iodoanilinium$^+$ cations were connected to the 18-crown-6 rings with 1:1 ratio by the N–H … O hydrogen bonds. The N–H … O hydrogen bonds show the N-O distance of 2.872–2.935 Å and N-H … O angle of 101.3–177.6°, respectively (Table 2), are in the normal ranges of typical N–H … O hydrogen bonds. The ClO_4^- anions in **1** display almost ordered and ideal tetrahedral geometry. The packing diagram for crystal **1** along $b + c$ axis is exhibited in Figure 2b, the perchlorate anions locate in the cavity of four adjacent [(4-Iodoanilinium)(18-crown-6)]$^+$ cations and link them with C-H … $O_{perchlorate}$ hydrogen bonds (C6-H6B … O5, C7-H7A … O5, C8-H8B … O7 and C10-H10A … O7, Table 2), which further stabilizes the supramolecular structure of crystal **1**. Furthermore, as checked by PLATON software, no C-H … π and π … π interactions existed in the supramolecular structure.

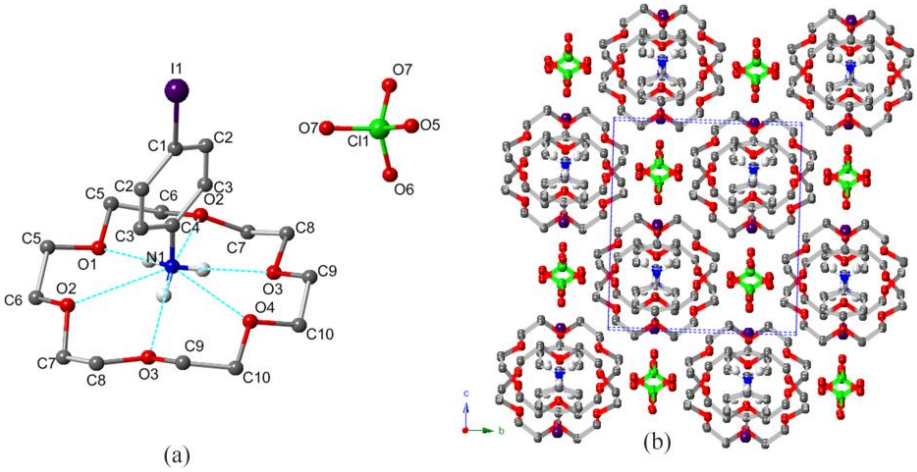

Figure 2. Crystal structure of crystal **1** at 153 K. (**a**) Asymmetric unit for crystal **1**, light blue dashed lines indicate the N-H … O hydrogen bonds; (**b**) Unit cell of crystal 1 viewed along the $b + c$ axis. Hydrogen atoms are omitted for clarity.

Table 2. Hydrogen bond lengths (Å) and bond angles (°) of **1** and **2**.

	D–H···A	d(D–H)	d(H···A)	d(D···A)	∠(D–H···A)
1	N1–H1B···O1	0.890	1.98	2.872	177.6
	N1–H1A···O2	0.890	2.56	2.9354	106.1
	N1–H1A···O3	0.890	1.99	2.872	174.5
	N1–H1A···O4	0.890	2.56	2.872	101.3
	C6-H6B . . . O5	0.990	2.65	3.449	137.73
	C7-H7A . . . O5	0.990	2.58	3.469	149.16
	C8-H8B . . . O7	0.990	2.67	3.603	156.76
	C10-H10A . . . O7	0.990	2.71	3.691	172.15
2	N1–H1B···O1	0.890	1.98	2.864	176.7
	N1–H1B···O2	0.890	2.58	2.9336	104.5
	N1–H1A···O3	0.890	1.99	2.8724	174.2
	N1–H1A···O4	0.890	2.57	2.878	101.4
	C6-H6B . . . F1	0.990	2.609	3.395	136.38
	C7-H7A . . . F1	0.990	2.530	3.408	147.54
	C8-H8B . . . F3	0.990	2.606	3.533	155.85

Besides, phase purities of the as-grown crystals were also checked by powder X-ray diffraction (XRD), as shown in Figure 3. The XRD patterns of crystals **1** and **2** at room temperature (298 K) matches well with the patterns simulated from the single-crystal structures measured at 153 K, except the peaks positions at 153 K were found to shift downward than those measured at room temperature, which compositing the regularity that the lattice parameters increased with the temperature increasing. In addition, the good matching of XRD patterns at the two temperatures, also confirm the thermal stability of crystals **1** and **2** in the temperature ranges of 153 K and 298 K. It is notable that at room temperature, the peaks intensities of crystal 2 are much stronger than those of crystal **1**, indicating the crystallinity of crystal **2** is better than crystal **1** at room temperature.

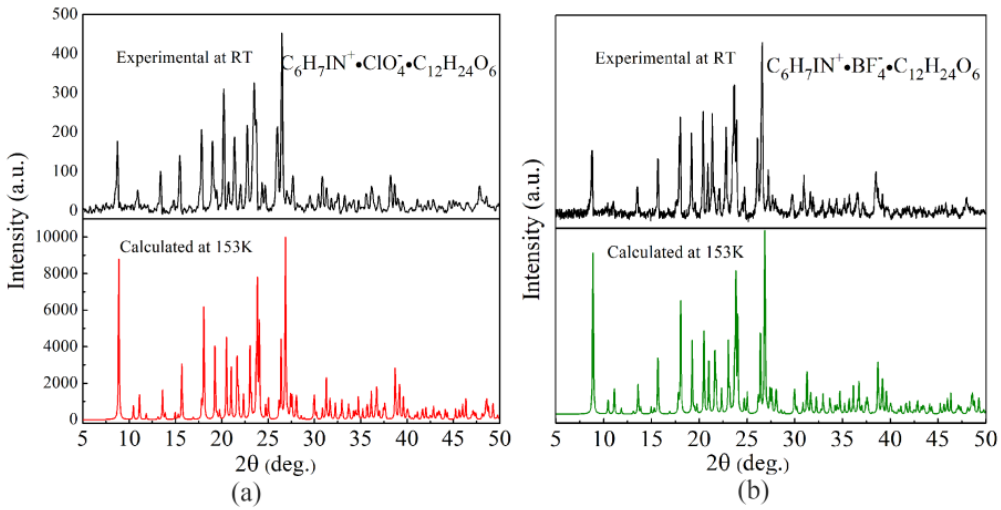

Figure 3. Calculated and experimental X-ray diffraction patterns of (**a**) crystal **1** and (**b**) crystal **2**.

3.3. Thermal Measurements

As depicted in Figure 4, the DSC and TG curves do not show any peak anomaly over the temperature ranges from −150 °C to 150 °C, indicating no phase transition was detected by thermal measurements in this temperature ranges, shown high thermal stability. To be precise, the phase decomposition temperatures are detected to be larger than 150 °C and 175 °C for **1** and **2**, respectively.

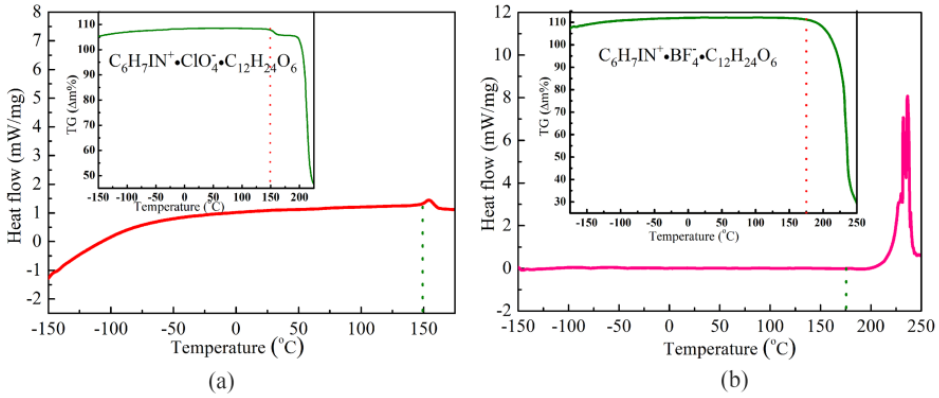

Figure 4. DSC and TG curves of (**a**) crystal **1** and (**b**) crystal **2**.

In addition, the phase transition temperatures and characteristics of a series of crown-ether-organic compounds are listed in Table 3. From Table 3, with the same organic amine and crown ether, the phase transition temperatures of tetrafluoroborate compounds demonstrated higher values than those of perchlorate compounds, which is likely related to the high boiling point of inorganic acid. It should be pointed out that although some possible factors, such as the boiling point of reactants, strength of electron absorption/ pushing effect of different substituents of organic amine, molecular weight and so on were compared, it is still difficult to estimate the thermal stability (phase transition temperature) or characteristic of crown-ether-organic compounds, due to there are so many numerous derivatives of organic amine (aniline, cyclamine and chain amine; and for same aniline and cyclamine, different quantities, kinds and positions of substituents). For example, the ferroelectric property was observed in 4-methoxyanilinium perrhenate 18-crown-6 [25] but was not detected in 4-ethoxyanilinium perchlorate 18-crown-6present [32], although the difference (methoxyl or ethyoxyl) of the two amine derivatives is very small.

Table 3. Phase transition temperatures and characteristics of a series of crown–ether–organic compounds.

Crystals	Phase Transition Temperature (K)	Characteristic
4-iodoanilinium perchlorate 18-crown-6 [this work]	423	High thermal stability; Narrow band gap (3.38 eV)
4-iodoanilinium borofluorate 18-crown-6 [this work]	448	High thermal stability; Narrow band gap (3.57 eV)
Cyclohexyl ammonium 18-crown-6 tetrafluoroborate [31]	397	Ferroelectric P_s = 3.27 μC/cm^2
Cyclohexyl ammonium 18-crown-6 perchlorate [31]	390	Ferroelectric P_s = 3.78 μC/cm^2
[(2,6-diisopropylanilinium)([18]crown-6)]BF_4] [27]	T_1 = 305 T_2 = 120	Ferroelectric P_s = 0.3 μC/cm^2
(2,6-diisopropylanilinium)([18]crown-6)](ClO_4) [26]	T_1 = 278 T_2 = 132	Ferroelectric P_s = 0.35 μC/cm^2
(4-nitroanilinium)$_2$(18-crown-6)$_2$(PF6)$_2$(CH3OH) [29]	265	- - - - -
(4-nitroanilinium)(18-crown-6)(HSO_4 [29]	255	- - - - -
Bis(imidazolium hydrochlorate) dehydrate 18-crown-6 [28]	220	Superior nonlinear optical switchingcontrast (~12); High laser-induced damage threshold (~8.9 GW/cm^2)
[(3-nitroanilinium$^+$)(18-crown-6)][IO_4](CH_3OH) [30]	220	- - - - -
4-ethoxyanilinium perchlorate 18-crown-6 [32]	163	- - - - -
Methoxyanilinium perrhenate 18-Crown-6 [25]	153	Ferroelectric P_s = 1.2 μC/cm^2
4-methoxyanilinium tetrafluoroborate-18-crown-6 [24]	127	Ferroelectric P_s = 0.54 μC/cm^2

- - - - -except phase transition, no characteristic was observed or reported.

3.4. Dielectric Properties

The temperature dependence ε' of crystals **1** and **2** taken at 1, 10, 100 and 500 kHz were illustrated in Figure 5. As can be seen, ε' were found to decrease with increasing frequency, especially at relative high temperatures, and no observable dielectric anomaly was observed in their measured temperature ranges.

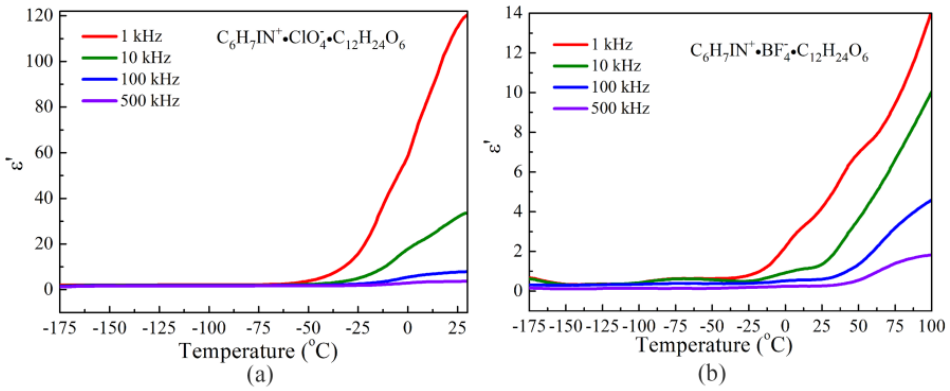

Figure 5. Dielectric constants of (**a**) crystal **1** and (**b**) crystal **2** as a function of temperature under a frequency ranges of 1 kHz to 500 kHz.

3.5. Optical Properties

The optical ultraviolet-visible absorption spectra were carefully performed to understand the optical and semiconducting properties, as shown in Figure 6. The absorption edges of compounds **1** and **2** located in ultraviolet ranges are assigned to 335 nm and 325 nm, respectively. The energy band gap E_g can be calculated by fitting the Tauc equation, and determined to be 3.38 eV and 3.57 eV, respectively, slightly smaller than those of layer perovskite $(benzylammonium)_2PbCl_4$ (3.65 eV) [3] and its analogues with the general formula $(R\text{-}NH_3)_2PbCl_4$ (3.64 eV) [35], and comparable to 3.20 eV for anatase-TiO_2 and 3.29 eV for ZnO. As it is known, a narrow energy band gap will be an advantage in optoelectronic application due to the expansion of active wavelength band.

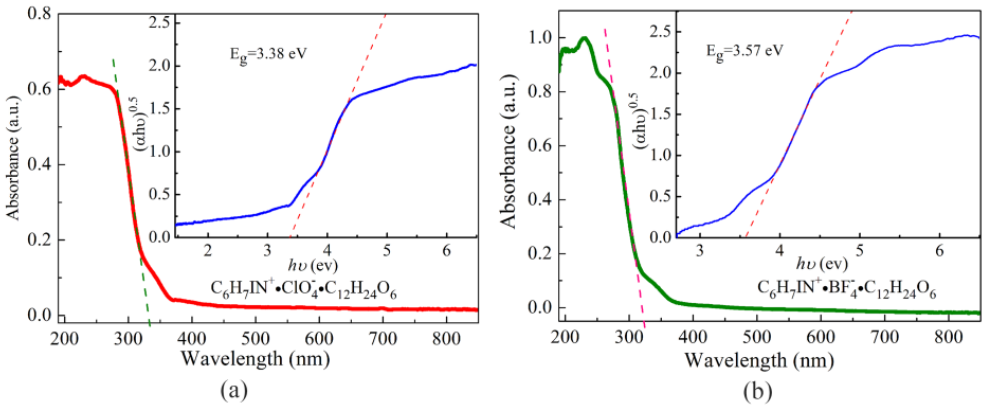

Figure 6. The optical ultraviolet-visible (vis) absorption spectra of (**a**) crystal **1** and (**b**) crystal **2**.

As illustrated in Figure 7a,b, the emission peaks appear at about 525 nm for compound **1**, and 425 nm and 550 nm for compound **2**. The intensities of emission peaks of **2** are slightly larger than that of **1**. The broad emission spectra (from 400 nm to 650 nm for both **1** and **2**) suggest that near-edge defect levels related to surface states take important part in the emission process [36].

Fitted by biexponential decay, the time-resolved PL decay curves of compounds **1** and **2** were calculated, as presented in Figure 7c,d. The faster decay time (τ_1) and slower decay time (τ_2) correspond to trap-assisted recombination on surface and free carrier recombination in bulk, respectively. From

decay curves, both faster and slower decay times of compound **1** were slightly longer than those of compound **2**.

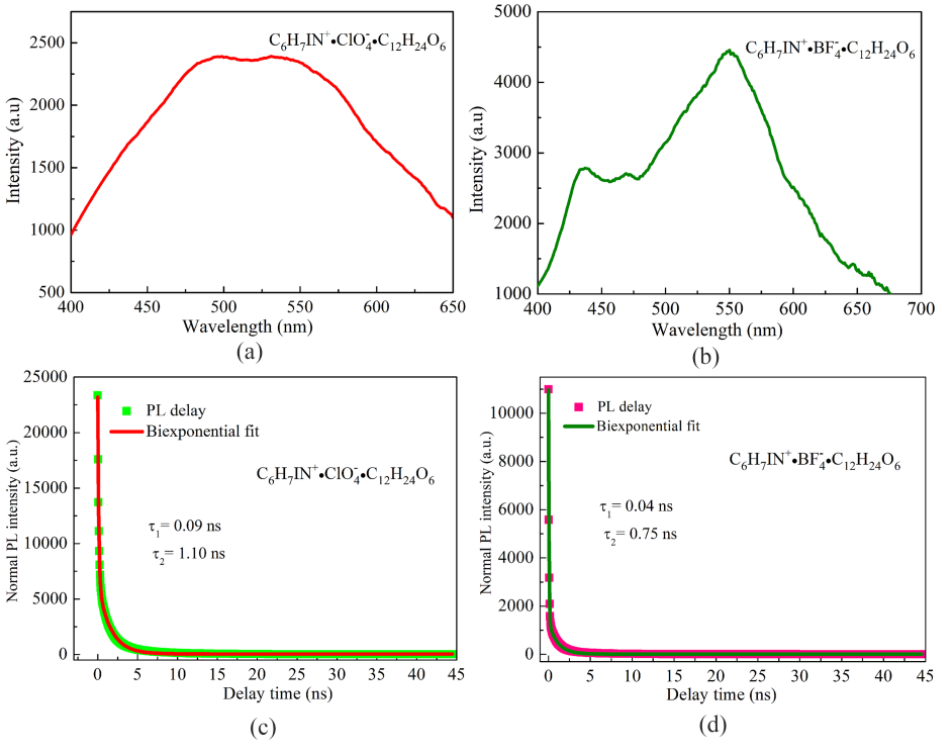

Figure 7. The PL spectra of (**a**) crystal **1** and (**b**) crystal **2**; The PL decay curves of (**c**) crystal **1** and (**d**) crystal **2**.

4. Discussion

Two organic–inorganic hybrid molecular crystals, $C_6H_7IN^+ \cdot ClO_4^- \cdot C_{12}H_{24}O_6$ and $C_6H_7IN^+ \cdot BF_4^- \cdot C_{12}H_{24}O_6$ were successfully grown by solution method. Their physical properties, including in structures, phase purities, thermal stability, absorption and fluorescence properties were systematically investigated for potential applications. Crystal structure analyses and thermal measurements showed compounds **1** and **2** exhibited similar crystal packings and maintain high thermal stability to 150 °C. The dielectric constants as a function of temperature were investigated, with no distinct dielectric constant anomaly were observed. For compounds **1** and **2**, the absorption edges located in ultraviolet ranges are assigned to 335 nm and 325 nm; the Eg were calculated to be 3.38 eV and 3.57 eV, respectively, slightly smaller than the data 3.65 eV of layer perovskite $(benzylammonium)_2PbCl_4$, indicating their potential applications in optoelectronic detection field. All the results throw light on the semiconductor properties of crown type compounds and provide two crown compounds with high thermal stability.

Author Contributions: L.Z. and T.K. are both the first authors, and they performed the experiments; F.Z. contributed in analysis of structures; D.W. and C.S. conceived and designed the experiments; C.S. wrote the paper; J.W. contributed in discussion of the results.

Funding: This research was funded by the National Natural Science Foundation of China (Grant No. 51602174, 51772172, 21601105 and 11847079) and Natural Science Foundation of Shandong Province (ZR2018BEM008).

Conflicts of Interest: The authors declare no conflicts of interest.

References

1. Ye, H.-Y.; Tang, Y.-Y.; Li, P.-F.; Liao, W.-Q.; Gao, J.-X.; Hua, X.-N.; Cai, H.; Shi, P.-P.; You, Y.-M.; Xiong, R.-G. Metal-free three-dimensional perovskite ferroelectrics. *Science* **2018**, *361*, 151–155. [CrossRef] [PubMed]

2. You, Y.-M.; Liao, W.-Q.; Zhao, D.; Ye, H.-Y.; Zhang, Y.; Zhou, Q.; Niu, X.; Wang, J.; Li, P.-F.; Fu, D.-W.; et al. An organic-inorganic perovskite ferroelectric with large piezoelectric response. *Science* **2017**, *357*, 306–309. [CrossRef] [PubMed]
3. Liao, W.-Q.; Zhang, Y.; Hu, C.-L.; Mao, J.-G.; Ye, H.-Y.; Li, P.-F.; Huang, S.D.; Xiong, R.-G. A lead-halide perovskite molecular ferroelectric semiconductor. *Nat. Commun.* **2015**, *6*, 7338. [CrossRef] [PubMed]
4. Zhang, W.-Y.; Ye, Q.; Fu, D.-W.; Xiong, R.-G. Optoelectronic duple bistable switches: A bulk molecular single crystal and unidirectional ultraflexible thin film based on imidazolium fluorochromate. *Adv. Funct. Mater.* **2017**, *27*, 1603945. [CrossRef]
5. Bermúdez-García, J.M.; Sánchez-Andújar, M.; Yáñez-Vilar, S.; Castro-García, S.; Artiaga, R.; López-Beceiro, J.; Botana, L.; Alegríade, A.; Señarís-Rodríguez, M.A. Multiple phase and dielectric transitions on a novel multi-sensitive [TPrA][M(dca)$_3$] (M: Fe^{2+}, Co^{2+} and Ni^{2+}) hybrid inorganic-organic perovskite family. *J. Mater. Chem. C* **2016**, *4*, 4889–4898.
6. Duong, T.-M.H.; Nobusue, S.; Tada, H. Face-shared structures of one-dimensional organic–inorganic lead iodide perovskites. *Appl. Phys. Express* **2018**, *11*, 115502. [CrossRef]
7. Uchida, H.; Oota, K.; Minami, T.; Takeya, K.; Kawase, K. Generation of single-cycle terahertz pulse using Cherenkov phase matching with 4-dimethylamino-N-methyl-4-stilbazolium tosylate crystal. *Appl. Phys. Express* **2017**, *10*, 062601. [CrossRef]
8. Jaffe, A.; Lin, Y.; Mao, W.L.; Karunadasa, H.I. Pressure-induced metallization of the halide perovskite (CH_3NH_3)PbI_3. *J. Am. Chem. Soc.* **2017**, *139*, 4330–4333. [CrossRef] [PubMed]
9. Kim, T.W.; Matsushita, T.; Uchida, S.; Kondo, T.; Segawa, H. Quantitative fraction analysis of coexisting phases in a polycrystalline $CH_3NH_3PbI_3$ perovskite. *Appl. Phys. Express* **2018**, *11*, 101401. [CrossRef]
10. Zhou, P.; Sun, Z.; Zhang, S.; Ji, C.; Zhao, S.; Xiong, R.-G.; Luo, J. A sequentially switchable molecular dielectric material tuned by the stepwise ordering in diisopropylammonium trifluoromethanesulfonate. *J. Mater. Chem. C* **2014**, *2*, 2341–2346. [CrossRef]
11. Tokizane, Y.; Nawata, K.; Han, Z.; Koyama, M.; Notake, T.; Takida, Y.; Minamide, H. Tunable terahertz waves from 4-dimethylamino-N-methyl-4-stibazolium tosylate pumped with dual-wavelength injection-seeded optical parametric generation. *Appl. Phys. Express* **2017**, *10*, 022101. [CrossRef]
12. Hoja, J.; Ko, H.-Y.; Neumann, M.A.; Car, R.; DiStasio, R.A., Jr.; Tkatchenko, A. Reliable and practical computational description of molecular crystal polymorphs. *Sci. Adv.* **2019**, *5*, eaau3338. [CrossRef] [PubMed]
13. Filippetti, A.; Caddeo, C.; Delugas, P.; Mattoni, A. Appealing perspectives of hybrid lead-Iodide perovskites as thermoelectric materials. *J. Phys. Chem. C* **2016**, *120*, 28472–28479. [CrossRef]
14. Sun, Z.; Tang, Y.; Zhang, S.; Ji, C.; Chen, T.; Hong, M.; Luo, J. Ultrahigh pyroelectric figures of merit associated with distinct bistable dielectric phase transition in a new molecular compound: di-n-Butylaminium trifluoroacetate. *Adv. Mater.* **2015**, *27*, 4795–4801. [CrossRef]
15. Wang, D.; Shen, C.; Lan, J.; Huang, P.; Cui, Z.; Kang, T.; Niu, Y.; Wang, S.; Wang, J.; Boughton, R.I. Exploration of the correlation between weak absorption and thermal-stress for KDP and 70%-DKDP crystals. *J. Alloys Compd.* **2019**, *790*, 212–220. [CrossRef]
16. Xia, Q.; Wang, H.; Huang, B.; Yuan, X.; Zhang, J.; Zhang, J.; Jiang, L.; Xiong, T.; Zeng, G. State-of-the-art advances and challenges of iron-based metal organic frameworks from attractive features, synthesis to multifunctional applications. *Small* **2018**, *15*, 1803088. [CrossRef]
17. Shen, C.; Wang, D.; Zhang, J.; Zhang, H.; Wang, J.; Boughton, R.I. The growth and investigations of electromechanical properties of Fresnoite $Ba_2Si_2TiO_8$ crystal as a function of orientation. *J. Cryst. Growth* **2018**, *487*, 17–22. [CrossRef]
18. Mączka, M.; Gągor, A.; Ptak, M.; Paraguassu, W.; da Silva, T.A.; Sieradzki, A.; Pikul, A. Phase transitions and coexistence of magnetic and electric orders in the methylhydrazinium metal formate frameworks. *Chem. Mater.* **2017**, *29*, 2264–2275. [CrossRef]
19. Shen, C.; Wang, D.; Zhang, H.; Wang, J.; Boughton, R.I. Fresnoite $Ba_2TiSi_2O_8$: A novel stimulated Raman scattering active crystal. *Appl. Phys. Express* **2016**, *9*, 122402. [CrossRef]
20. Shi, C.; Zhang, X.; Yu, C.-H.; Yao, Y.-F.; Zhang, W. Geometric isotope effect of deuteration in a hydrogen-bonded host-guest crystal. *Nat. Commun.* **2018**, *9*, 481. [CrossRef]

21. Mączka, M.; Costa, N.L.M.; Gągor, A.; Paraguassu, W.; Sieradzkic, A.; Hanuzad, J. Structural, thermal, dielectric and phonon properties of perovskite-like imidazolium magnesium formate. *Phys. Chem. Chem. Phys.* **2016**, *18*, 13993–14000. [CrossRef]
22. Dufrois, Q.; Daran, J.-C.; Vendier, L.; Dinoi, C.; Etienne, M. Triangles and squares for a unique molecular crystal structure: unsupported two-coordinate lithium cations and CC agostic interactions in cyclopropyllithium derivatives. *Angew. Chem.* **2018**, *130*, 1804–1809. [CrossRef]
23. Fu, D.-W.; Cai, H.-L.; Li, S.-H.; Ye, Q.; Zhou, L.; Zhang, W.; Zhang, Y.; Deng, F.; Xiong, R.-G. 4-Methoxyanilinium perrhenate 18-Crown-6: A new ferroelectric with order originating in swing like motion slowing down. *PRL* **2013**, *110*, 257601. [CrossRef] [PubMed]
24. Fu, D.-W.; Zhang, W.; Cai, H.-L.; Zhang, Y.; Ge, J.-Z.; Xiong, R.-G.; Huang, S.D. Supramolecular bola-like ferroelectric: 4-methoxyanilinium tetrafluoroborate-18-crown-6. *J. Am. Chem. Soc.* **2011**, *133*, 12780–12786. [CrossRef] [PubMed]
25. Shen, C.; Wang, D.; Xu, H.; Pan, Z.; Zhang, H.; Wang, J.; Boughton, R.I. Bulk crystal growth and thermal, spectroscopic and laser properties of disordered Melilite Nd:$Ca_2Ga_2SiO_7$ single crystal. *J. Alloys Compd.* **2017**, *727*, 8–13. [CrossRef]
26. Zhang, Y.; Ye, H.-Y.; Fu, D.-W.; Xiong, R.-G. An order-disorder ferroelectric host-guest inclusion compound. *Angew. Chem. Int. Ed.* **2014**, *53*, 2114–2118. [CrossRef]
27. Ye, H.-Y.; Li, S.-H.; Zhang, Y.; Zhou, L.; Deng, F.; Xiong, R.-G. Solid state molecular dynamic investigation of an inclusion ferroelectric: [(2,6-Diisopropylanilinium)([18]crown-6)]BF_4. *J. Am. Chem. Soc.* **2014**, *136*, 10033–10040. [CrossRef] [PubMed]
28. Sun, Z.; Li, S.; Zhang, S.; Deng, F.; Hong, M.; Luo, J. Second-order nonlinear optical switch of a new hydrogen-bonded supramolecular crystal with a high laser-induced damage threshold. *Adv. Opt. Mater.* **2014**, *2*, 1199–1205. [CrossRef]
29. Chen, Y.; Liu, Y.; Gao, B.; Zhu, C.; Liu, Z. Inorganic anions regulate the phase transition in two organic cation salts containing $[(4\text{-nitroanilinium})(18\text{-crown-6})]^+$ supramolecules. *Crystals* **2017**, *7*, 224. [CrossRef]
30. Liu, Z.-Q.; Liu, Y.; Chen, Y.; Zhao, W.-Q.; Fang, W.-N. Synthesis, characterization, and phase transition of an inorganic-organic hybrid compound, [(3-nitroanilinium+)(18-crown-6)][IO_4−](CH_3OH). *Chinese Chem. Lett.* **2017**, *28*, 297–301. [CrossRef]
31. Tang, Y.-Z.; Yu, Y.-M.; Xiong, J.-B.; Tan, Y.-H.; Wen, H.-R. Unusual high-temperature reversible phase-transition behavior, structures, and dielectric–ferroelectric properties of two new crown ether clathrates. *J. Am. Chem. Soc.* **2015**, *137*, 13345–13351. [CrossRef]
32. Ge, J.-Z.; Fu, X.-Q.; Hang, T.; Ye, Q.; Xiong, R.-G. Reversible phase transition of the 1:1 complexes of 18-crown-6 with 4-ethoxyanilinium perchlorate. *Cryst. Growth Des.* **2010**, 3632–3637. [CrossRef]
33. Ge, J.-Z.; Zhao, M.-M. 4-Methylanilinium tetrafluoroborate 18-crown-6 clathrate. *Acta Cryst. E* **2010**, *66*, o1478. [CrossRef] [PubMed]
34. Zhang, Y.; Zhao, M.-M. Accelerating ab initio phasing with de novo models. *Acta Cryst. E* **2011**, *67*, o596. [CrossRef] [PubMed]
35. Zhang, S.; Audebert, P.; Wei, Y.; Lauret, J.-S.; Galmichec, L.; Deleporte, E. Synthesis and optical properties of novel organic-inorganic hybrid UV $(R\text{-}NH_3)_2PbCl_4$ semiconductors. *J. Mater. Chem.* **2011**, *21*, 466–474. [CrossRef]
36. Ding, J.; Du, S.; Zhao, Y.; Zhang, X.; Zuo, Z.; Cui, H.; Zhan, X.; Gu, Y.; Sun, H. High-quality inorganic-organic perovskite $CH_3NH_3PbI_3$ single crystals for photo-detector applications. *J. Mater. Sci.* **2017**, *52*, 276–284. [CrossRef]